



# Steady State Ceiling Jet Behavior under an Unconfined Ceiling with Beams

Vahid Motevalli\*, *School of Engineering and Applied Science,  
The George Washington University, 801 22nd Street, NW, Washington,  
DC 20052, USA*

Zheng P. Yuan, *CADfps, LLC, Houston, USA*

**Abstract.** Smooth horizontal and sloped ceiling jets have been studied extensively. The characteristics of these jets, i.e., temperature and velocity profiles, have been defined previously, particularly for horizontal ceilings. The presence of beams and obstructions pose a real challenge for both modeling and detector placement procedures. The present paper reports temperature profiles of ceiling jets for horizontal beamed ceilings, within beamed spaces that do not contain the plume impingement point. Furthermore, these results apply to an unconfined ceiling corresponding to large spaces or long enclosures where the end walls are far away. The research results can be highly useful for prediction of temperature of ceiling jet flows for spaces with continuous beams or joists, but may also be useful for other types of obstructions such as long light fixtures as well as smoke curtains in high bay areas. The correlation developed for temperature distribution within the bays of the beamed ceiling is based on the beam depth to ceiling height and is referenced to the smooth ceiling correlation developed by Motevalli. All data has been obtained from scaled experiments for non-dimensional fire sizes ranging from 0.0024 to 0.035. This range corresponds to fires from 38 kW to 560 kW for a 3 m ceiling height.

**Keywords:** ceiling jet, smooth, horizontal, beam, obstruction, heat detection, sprinkler activation, scale modeling, fire induced flows

## Nomenclature

$c_p$	constant pressure heat capacity, kJ/(kg K),
$d$	beam depth, m,
$g$	acceleration of gravity, m/s <sup>2</sup> ,
$H$	ceiling height, m,
$l_b$	distance to ceiling beam from center of bay, m,
$l_T$	Gaussian thermal thickness, m,
$\dot{Q}$	heat release rate kW,
$\dot{Q}^*$	non-dimensional convective heat release rate,
$\dot{Q}_c$	convective heat release rate, $Q_c = (1 - \gamma_r)Q$ , kW,
$r$	radial position, m,
$T_\infty$	ambient temperature, K,
$w$	beam width, m,

\* Correspondence should be addressed to: Vahid Motevalli, E-mail: vahidm@gwu.edu

$X$	location on $x$ -axis, $X = r \sin(\alpha)$ , m,
$Y$	location on $y$ -axis, $Y = r \cos(\alpha)$ , m,
$z$	distance below ceiling, m,
$\Delta T$	excess temperature, °C,
$\Delta T^*$	non-dimensionalized temperature,
$\Delta T(r, \alpha)_b$	excess temperature of beamed ceiling jet, °C,
$\Delta T(r, \alpha)_{\max, b}$	maximum excess temperature of beamed ceiling jet, °C,
$\Delta T(r, \alpha)_{\max, s}$	maximum excess temperature of smooth ceiling jet, °C,
$\Delta T(r)_s$	excess temperature of smooth unconfined ceiling jet, °C,
$\alpha$	angle of radial line with beam, degree,
$\gamma_r$	radiative fraction,
$\theta$	non-dimensional temperature,
$\theta_{\max}$	non-dimensional maximum temperature

## 1. Introduction

There are building constructions where many detectors and sprinklers are installed on ceilings with beams or other obstructions. Ceiling obstructions make ceiling jet flow complicated, and temperature and velocity profiles under these conditions are not fully characterized. Recent works in CFD simulation have made a lot of progress in understanding the complex ceiling jet flows [1, 2]. However, it is difficult to fully validate these models and they are still too complex to be used for engineering design and assessment.

Current practices and the NFPA standards [3–5] do not provide access to the necessary engineering information to address obstructed ceiling jets. This work attempts to provide some of the basic information needed to enhance the current practices. Previously, other researchers have also addressed these flows [6–11]. The complexity of this problem has restricted the applicability of the results to a limited number of ceiling configurations. Normally, multiple beams exist and construct multiple channels on the ceiling, and detectors or sprinklers may be installed at positions within a bay not containing the initial fire plume. In this work, the beamed ceiling jet temperature profile was investigated for multiple beam spacing in the midline of the secondary bay and an empirical correlation has been developed for the maximum temperature variations. The temperature and velocity profiles for beamed ceiling jet flows are functions of the fire size and geometric variables associated with beams and ceilings. These geometric variables include the beam width,  $w$ , beam depth,  $d$ , beam spacing,  $2l_b$ , and ceiling height,  $H$  (see Figure 1). It is important to define key regions of the flow in this arrangement. The primary bay or channel is the region between two ceiling beams where the fire plume impinges. The secondary bay is the bay adjacent to the primary bay. Both the primary and secondary bays are illustrated in Figure 2.

This work expands on the previous research performed by Koslowski and Motevalli [12], who reported an empirical correlation validated for the flow within the secondary bay at locations perpendicular to the beam. No correlations for the beamed ceiling jet temperature and velocity on the midline within the secondary channel have been developed previously. For design purposes, the parameters of the experimental research are limited. Heat detector and sprinkler placement is

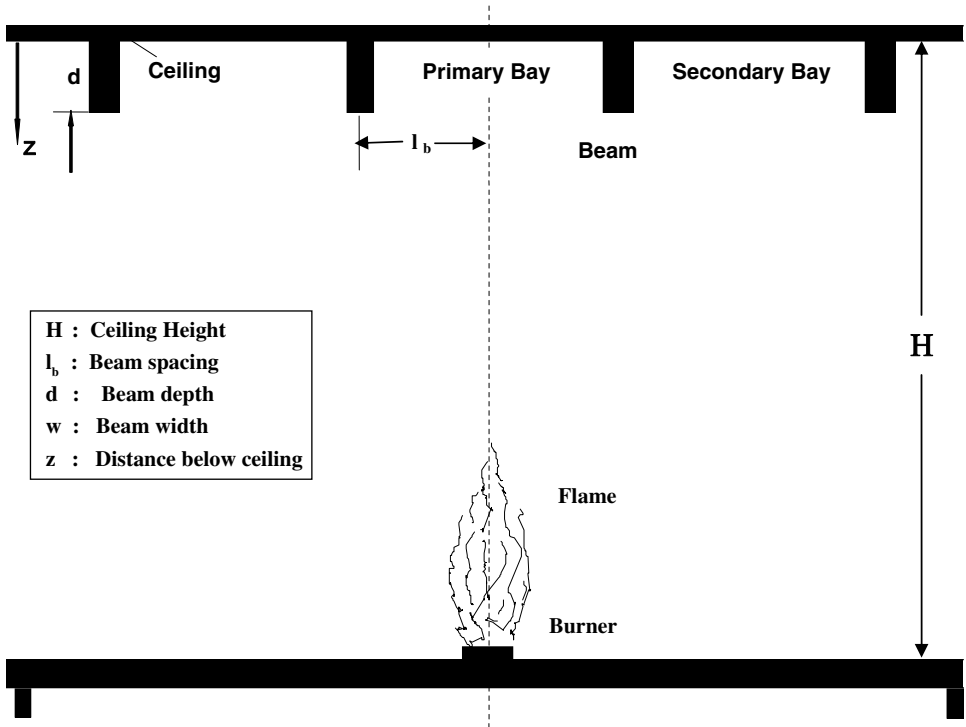


**Figure 1. Schematic of the beamed ceiling jet simulation apparatus.**

typically at center of bays or under the beams. For design considerations, placement of detectors & sprinklers below the beam normally does not pose a problem as actuation would often happen more readily below the beam regardless of fire location being directly below the beam or not.

## 2. Theory and Approach

The temperature correlations for the smooth ceiling jet can be expressed as a function of ceiling configuration, i.e., height, distance from plume axis and convective heat release rate. Similarly, the temperature correlation for beamed ceiling jet can also be expressed in terms of the geometric variables of a beamed ceiling, such as beam depth, width and spacing, (shown via dimensional analysis by Koslowski and Motevalli [12]) these geometric variables of the beamed ceiling are shown in Figure 1. The ceiling jet temperature for a smooth, horizontal and unconfined ceiling jet is a function of the radial position,  $r$ , the ceiling height,  $H$ , and the non-dimensional fire size,  $\dot{Q}^*$ . The scaling laws referred to here are based on Froude modeling and their accuracy in representing large-scale fire-induced flows have been well-established with very good results when implemented carefully and with noted limitations. Quintiere has described the applicability of small-scale experiments and the validity of scaling laws in a comprehensive review paper [13].

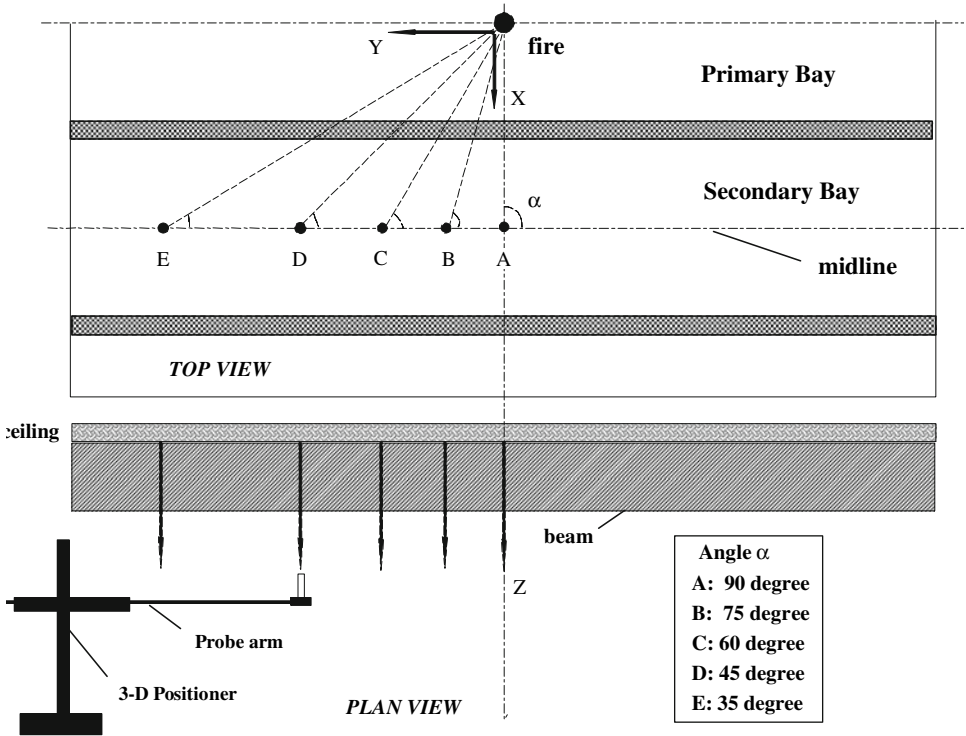


**Figure 2. Plane top view and side views (bottom) of the experimental configuration defining terms and measurement points.**

Based on the scaling laws, for steady fires, the ceiling jet maximum temperature can be expressed by:

$$\Delta T_{\max,s}^* = F\left(\frac{r}{H}, \dot{Q}^*\right) \tag{1}$$

where subscript “max, s” refers to a maximum value for a smooth ceiling condition.

In general, the temperature difference  $\Delta T$  for a ceiling jet can be non-dimensionalized by the following form:

$$\Delta T^* = \frac{\Delta T}{\dot{Q}^{*2/3} T_\infty} \tag{2}$$

where,  $T_\infty$  is the absolute ambient temperature.

According to non-dimensionalization methods and as described by Motevalli [14], the maximum temperature for smooth unconfined ceiling can be depicted as follows:

$$\Delta T(r)_{\max,s} = \Delta T_{\max,s}^* \dot{Q}^{*\frac{2}{3}} T_{\infty} \quad (3)$$

where

$$\dot{Q}^* = \frac{\dot{Q}_c}{(c_p \rho_{\infty} T_{\infty} \sqrt{g} H^{2.5})} \quad (4)$$

and correlation reported by Motevalli and Marks [15] is noted below:

$$\Delta T_{\max,s}^* = 0.166 \left(\frac{r}{H}\right)^{-2} + 1.2 \left(\frac{r}{H}\right)^{-1} + 2.0 \quad 0.26 \leq \frac{r}{H} \leq 1.0 \quad (5)$$

Note that  $\dot{Q}_c$  is the convective heat release rate, i.e.,  $\dot{Q}_c = \dot{Q}_{tot} - \dot{Q}_r$ , where  $\dot{Q}_r$  is the radiative loss.

Motevalli and Marks [15] further defined the ceiling jet temperature profile by the following:

$$\frac{\Delta T(r)_s}{\Delta T(r)_{\max,s}} = 4.24 \left(\frac{z}{l_T} + 0.094\right)^{0.755} e^{[-2.57(\frac{z}{l_T})]} \quad 0.26 \leq \frac{r}{H} \leq 2.0 \quad (6)$$

where the non-dimensional ceiling jet thermal Gaussian thickness,  $l_T$ , is defined by:

$$\frac{l_T}{H} = 0.112 \left(1 - e^{[-2.24(\frac{z}{H})]}\right) \quad (7)$$

Although correlations 5–7 are based on small-scale experiments and for weak plume range, Motevalli and Marks [15] compared them with large-scale correlations and showed that if one can quantify the convective heat release rate of large-scale fire experiments accurately, then reasonably good agreement is obtained. Additionally, small-scale correlation of Motevalli and Marks offer a correlation for temperature profile which large-scale experiments lack. Using dimensional analysis, the maximum temperature of the unconfined beamed ceiling jet flow within a secondary channel can be described by:

$$\Delta T(r, \alpha)_{\max,b} = F\left(\frac{X}{H}, \frac{Y}{H}, \frac{w}{H}, \frac{d}{H}, Q^*\right) \quad (8)$$

where subscript,  $b$ , refers to the beamed ceiling.

Since  $X = 2l_b$  and  $Y = 2l_b/\tan(\alpha)$ , Equation (8) can also be rewritten as follow:

$$\Delta T(r, \alpha)_{\max,b} = F\left(\frac{l_b}{H}, \frac{w}{H}, \frac{d}{H}, \frac{\alpha}{90}, Q^*\right) \quad (9)$$

Here,  $\alpha$  is being used as a convenient way to identify the location of interest within a bay.

Following the approach taken by Koslowski and Motevalli [12, 17], the beamed ceiling jet temperature can be related to the smooth ceiling jet in the following normalization:

$$\theta = \frac{\Delta T_b^*}{\Delta T_s^*} \quad (10)$$

Equation (10), along with the previous relations, allows the analysis of the scaled experiments. The non-dimensional temperature,  $\theta$ , is in general form and can be expressed as  $\theta_{\max} = \Delta T_{b,\max}^* / \Delta T_{\max}^*$ . The range of  $\theta$  is between horizontal smooth ceiling (no beam,  $\theta = 1.0$ ) to some upper limit of beam depth ( $d$ ), which would make the flow approach a corridor flow. For a corridor flow,  $\theta$  would approach zero when there is no spillage from the primary channel into the secondary channel.

### 3. Experiment

The Beamed Ceiling Jet Simulation Apparatus and other related equipment were developed previously [12] and experiments were performed at the Fire Science and Combustion Laboratory at Worcester Polytechnic Institute (WPI) [16] and are fully described including burner size, etc. in these references. The experiments, listed in Table 1, were designed to maximize the range of  $\dot{Q}^*$ ,  $w/d$ ,  $l_b/H$ ,  $d/H$  and  $\alpha/90$  being tested. The non-dimensional heat release rate,  $\dot{Q}^*$ , ranging from 0.0024 to 0.0351 corresponds to fire sizes ranging from 38 kW to 560 kW in a 3.0 m high room. This provides a large range that covers plume strength beyond weak plume range.

**Table 1**  
**Experimental Parameters [16]**

No.	$Q$ (kW)	$\dot{Q}^*$	$H$ (m)	$l_b$ (m)	$w$ (m)	$d$ (m)	$d/H$	$l_b/H$
1	5.0	0.0153	0.60	0.30	0.04	0.15	0.25	0.50
2	10.0	0.0293	0.60	0.30	0.04	0.15	0.25	0.50
3	10.0	0.0245	0.65	0.30	0.04	0.15	0.23	0.46
4	10.0	0.0167	0.75	0.30	0.04	0.15	0.20	0.40
5	5.0	0.0088	0.75	0.25	0.04	0.09	0.12	0.33
6	5.0	0.0091	0.75	0.25	0.04	0.04	0.05	0.33
7	5.0	0.0042	1.00	0.30	0.04	0.15	0.15	0.30
8	10.0	0.0082	1.00	0.30	0.04	0.15	0.15	0.30
9	10.0	0.0084	1.00	0.25	0.04	0.09	0.09	0.25
10	5.0	0.0043	1.00	0.25	0.04	0.09	0.09	0.25
11	10.0	0.0049	1.25	0.25	0.04	0.09	0.07	0.20
12	5.0	0.0024	1.25	0.25	0.04	0.04	0.03	0.20
13	5.0	0.0043	1.00	0.25	0.08	0.09	0.09	0.25
14	5.0	0.0088	0.75	0.30	0.04	0.09	0.12	0.40
15	10.0	0.0351	0.57	0.23	0.04	0.04	0.07	0.40

In addition, use of premixed methane-air flame ensured accurate measurements of convective heat release rate to within  $\pm 3\%$ . In each experiment, steady state temperature data were collected at five different positions on the midline of the secondary bay corresponding to angles of 90, 75, 60, 45, and 35 degrees measured with respect to the centerline of the primary bay (see Figure 2). These points correspond to positions  $Y$  along the midline of the secondary bay such that  $\tan(\alpha) = X/Y$ . Locating of the probes horizontally were done within an accuracy of 0.01 m and vertically to within 0.001 m. In order to examine the effect of geometric variables on the ceiling jet flow according to Equation (9), and the heat release rate, a matrix of experiments shown in Table 1 was developed. Temperature data were collected over 10 s interval at 15 vertical positions below the ceiling corresponding to:  $z = 0, 5, 10, 15, 20, 30, 40, 50, 60, 75, 90, 105, 120, 140, 160$  mm ( $\pm 1$  mm). The experiments were all started at  $t = 0$  with ambient laboratory conditions when flame was ignited. The ceiling was unconfined and insulated on top (simulating adiabatic conditions) and was painted black to an emissivity of approximately one.

A 0.0254 mm (0.001") diameter E type (chromel-constantan) thermocouple was employed to collect the temperature data. The probe could be moved both horizontally and vertically using a sliding motor-driven mechanism. The probe was connected to the data acquisition system with a pair of insulated and shielded cable to reduce the noise level. A program written in the BASIC language was used with a Metro byte data acquisition system to collect the data.

## 4. Results and Analysis

### 4.1. Temperature Profiles

Temperature profiles at the midline within the secondary channel were measured with a variety of multiple beam spacings, beam widths, beam depths, ceiling heights, and fire sizes as described in Table 1. Previous studies reviewed by Koslowski and Motevalli [12, 17] and their experimental results indicates that the width of the obstruction,  $w$ , (when of the same order of magnitude or less, as the beam depth,  $d$ ) is not a significant parameter. In order to further examine this hypothesis, the temperature profiles at two locations along the secondary bay centerline. ( $\alpha = 90^\circ$  &  $\alpha = 45^\circ$ ) are shown in Figures 3 and 4, while all fire and ceiling variables are kept the same except  $w/d$  ratio, which is varied by a factor of 2. Clearly, the effect is not observable within our experimental resolution. In all figures, the smooth-unconfined horizontal ceiling jet non-dimensional temperature profile [15] is plotted for reference.

A similar comparison examining the effect of beam spacings,  $l_b$ , on the ceiling jet temperature profile is shown in Figures 5 and 6. Effect of variation in  $l_b/H$  is less than 10%. Although, the variation of  $l_b/H$  in these cases is not large, these spacing fall within most practical ranges. The beam spacing effect may become significant in special cases. It is also interesting to note that for the beam depth of Figures 5 and 6 (i.e.,  $d/H = 0.12$ ) a clear 1-dimensional flow within the bay confinement has developed where the temperature profiles are initially flat, for  $z$  less than the beam depth.

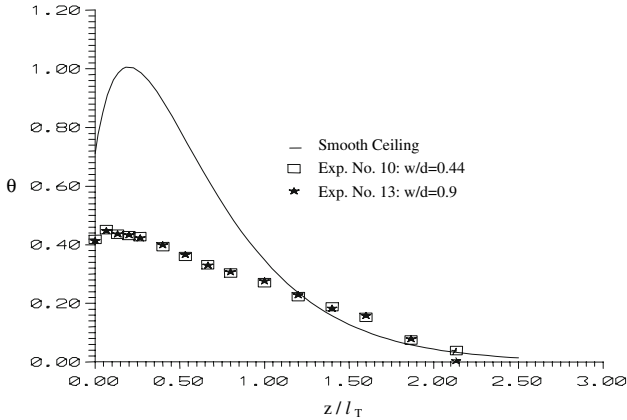


**Figure 3. Non-dimensional temperature profiles at 90-degree positions,  $Q = 5.0$  kW,  $H = 1.00$  m,  $d/H = 0.09$ .**

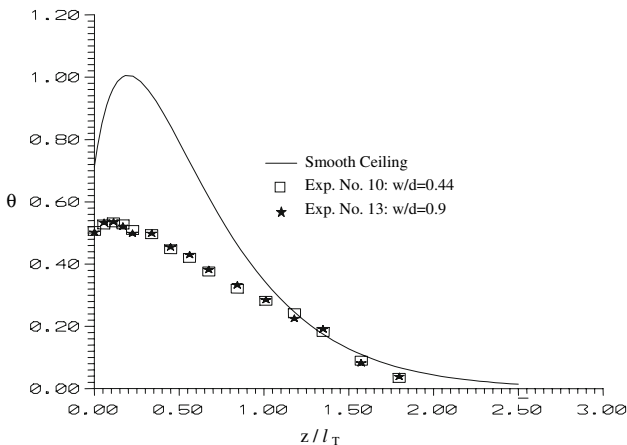


**Figure 4. Non-dimensional temperature profiles at 45-degree positions, effect of beam width;  $Q = 5.0$  kW,  $H = 1.00$  m,  $d/H = 0.09$ .**

As previous researchers have determined [10–12], the beams certainly reduce the temperature of the ceiling jet within the secondary channel. Comparison of temperature profiles for different  $d/H$  values are shown in Figures 7 and 8, where only  $\alpha$  is varied in the two figures. Clearly, with decreasing  $\alpha$ , each non-dimensional temperature profile of beamed ceiling jet at a given  $d/H$  becomes steeper and is closer to that of the smooth unconfined ceiling. Therefore, temperature profiles are mainly affected by  $d/H$  and  $\alpha/90$ . The gradient of ceiling jet temperature profile reduces significantly as  $d/H$  is increased. The uniform temperature near the ceiling, at  $\alpha/90 \approx 1$ , is caused by large vortices being shed and recirculation regions when  $d/H$  is increased. This is slightly more evident for  $\alpha = 90^\circ$  (Figure 7) since



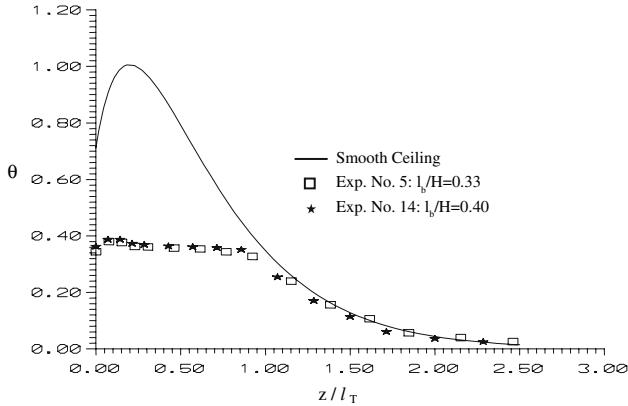


**Figure 5. Non-dimensional temperature profiles at 90-degree positions, effect of beam spacing;  $Q = 5.0$  kW,  $H = 0.75$  m,  $d/H = 0.12$ .**

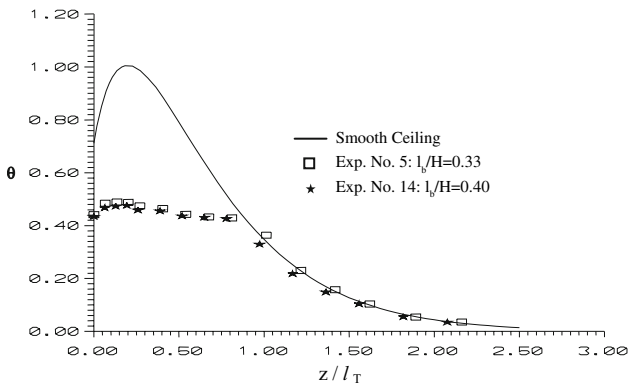


**Figure 6. Non-dimensional temperature profiles at 45-degree positions, effect of beam spacing,  $Q = 5.0$  kW,  $H = 0.75$  m,  $d/H = 0.12$ .**

ceiling jet flow is perpendicular to the beam. Along the secondary bay, flow develops and temperature profile shape becomes more pronounced. It is observed that regardless of the variation in geometry, ceiling height, and fire size, the secondary bay ceiling jet temperature is significantly lower than the smooth ceiling jet temperature for  $d/H$  greater than 0.03. This has an important effect on actuation time of heat detectors and sprinklers for minor obstructions.

In Figure 9, the locations of crossing points between the smooth ceiling jet temperature profiles ( $d/H = 0$ ) and beamed ceiling jet temperature profiles also points to the development of corridor type flows. This crossing is pronounced for results bracketed by,  $0.07 \leq d/H \leq 0.09$ , and they seem to be at vertical distances,  $z \approx d$ . For example, in Figures 3, 4, 7 and 8, the crossing points are located within  $0.8 \leq z/l_T \leq 1.2$ . The distance  $z$  can be determined and are approximately equal

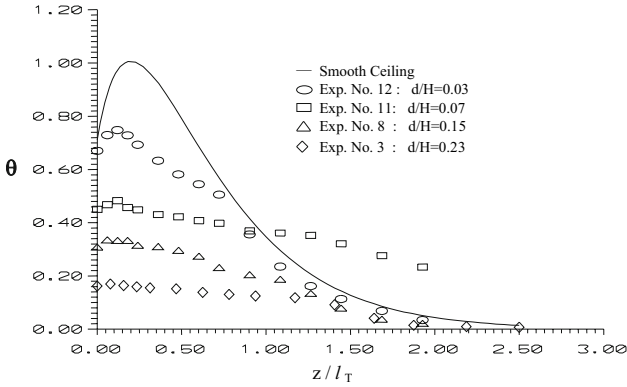


**Figure 7. Non-dimensional temperature profiles along the secondary bay demonstrating corridor flow effect,  $\alpha = 90^\circ$ .**

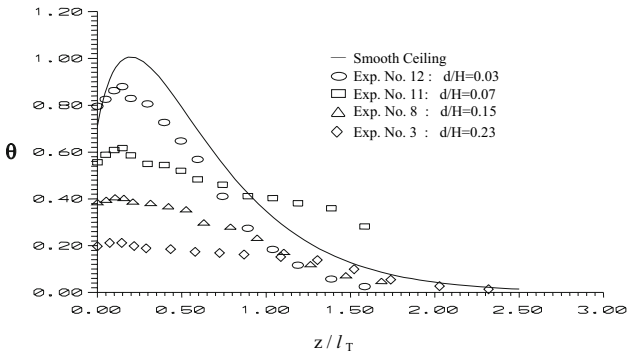


**Figure 8. Non-dimensional temperature profiles along the secondary bay demonstrating corridor flow effect,  $\alpha = 45^\circ$ .**

to the beam depth for each condition. For  $\alpha = 90$  (perpendicular flow to the beam),  $r/H = 2l_b/H$ , applying this condition to Equation (7) shows that for  $0.2 \leq l_b/H \leq 0.5$ ,  $l_T/H$  varies between 0.07 to 0.1. Therefore,  $z/l_T = 1.0$  (ratio of thermal Gaussian thickness,  $l_T$ , to the ceiling height,  $H$ ) is approximately close to  $d/H = 0.1$ . This means that the ceiling jet flow with temperature less than 37% of the maximum value is flowing to the secondary bay. This percentage is further reduced at lower  $\alpha$  as also demonstrated in Figures 9 and 10. Examination of our experimental data showed that the temperature profile becomes increasingly uniform for  $d/H > 0.03$  since the ceiling jet impinges on the beam and the flow is directed downward. This effect on the temperature profile can be ascribed to the redirection of the ceiling jet flow under the beam. Koslowski and Motevalli addressed this phenomenon and showed the transition to be evident for  $0.06 \leq d/H \leq 0.09$  [17]. For lower  $d/H$  values, the corridor flow does not fully develop and the temperature profile retains a form similar to the smooth ceiling jet case. For

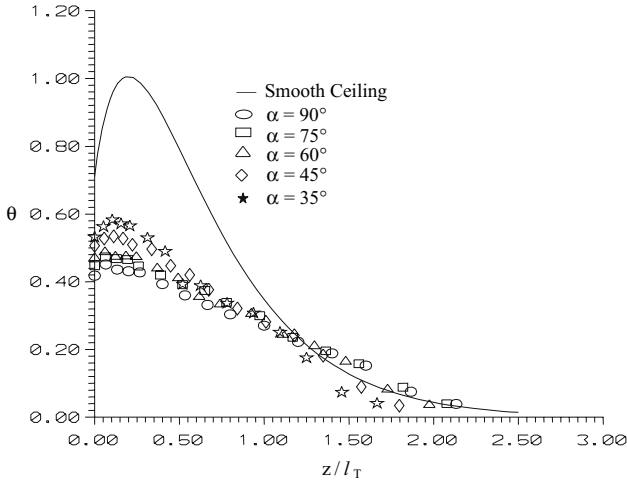


**Figure 9. Non-dimensional temperature profiles,  $H = 1.0$  m,  $Q = 5$  kW,  $d/H = 0.09$  and  $l_b/H = 0.25$ .**

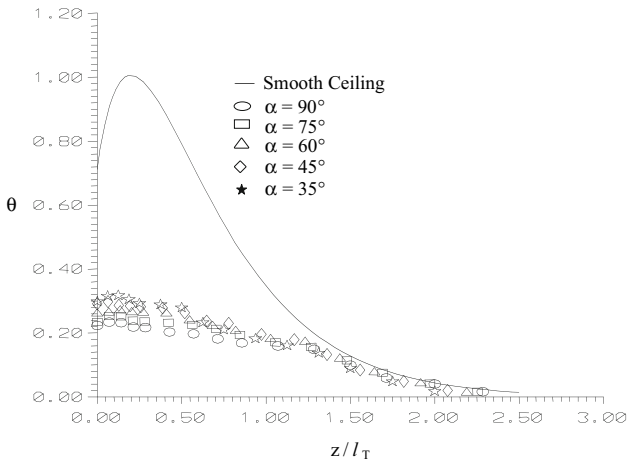


**Figure 10. Non-dimensional temperature profiles,  $H = 0.75$  m,  $Q = 10$  kW,  $d/H = 0.2$  and  $l_b/H = 0.4$ .**

larger  $d/H$  values, development of the corridor flow makes the temperature profiles more uniform along with the reduction of temperature and prevents the crossing of the smooth ceiling jet temperature profile (see Figures 7 and 8).

#### 4.2. Maximum Temperatures

The data from experiments 1–15 involve a wide range of non-dimensional fire sizes, beam widths, beam spacing, beam depths and ceiling heights. Despite these

variations, non-dimensional maximum temperature can be reasonably considered as a function of  $d/H$  and  $\alpha/90$ . The normalized data were analyzed to determine a polynomial fit shown in Equation (11).

$$\theta_{\max} = [a_0 + a_1 \left(\frac{d}{H}\right) + a_2 \left(\frac{d}{H}\right)^2 \dots][b_0 + b_1 \left(\frac{\alpha}{90}\right) + b_2 \left(\frac{\alpha}{90}\right)^2 + \dots] \quad (11)$$

The constants in the above two sub-polynomials have been obtained by using a modified Levenberg-Marquardt algorithm and a finite-difference Jacobia [18] to solve for this nonlinear least square fit. The constants obtained are:

$$\begin{aligned} \bar{a}_0 &= 0.417, a_1 = -4.148, a_2 = 23.493, a_3 = -51.718, b_0 = 3.899, \\ b_1 &= -3.021, b_2 = 1.381 \end{aligned}$$

The goodness of this fit is determined by the correlation coefficient defined in a standard fashion [18]. This correlation has a 0.995 coefficient and is plotted in Figure 11 and seems to fit the experimental data very well for the  $0.03 \leq d/H \leq 0.25$ . In Figure 11,  $f(\alpha)$  was determined by calculation of  $\theta_{\max}$  using Equation (11) at different ( $\alpha$ ) resulting in the following relation:

$$f(\alpha) = 3.90 - 3.02 \left(\frac{\alpha}{90}\right) + 1.38 \left(\frac{\alpha}{90}\right)^2 \quad (12)$$

Finally combining Equations (11) and (12) the following equation is obtained:

$$\frac{\theta_{\max}}{f(\alpha)} = 0.42 - 4.15 \left(\frac{d}{H}\right) + 23.49 \left(\frac{d}{H}\right)^2 - 51.72 \left(\frac{d}{H}\right)^3 \quad (13)$$

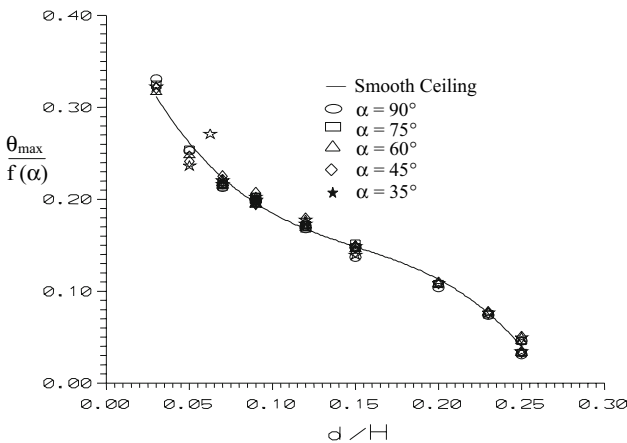


**Figure 11. Comparison of experimental data for all measured positions within the secondary bay with the formulated correlation.**

The significance of the analysis and correlation developed (Equation 13), which is shown in Figure 11 is that all the data are collapsed for the entire range of  $d/H$ , various  $l_b/H$  and  $\dot{Q}^*$ . The correlation behaves physically correct. As  $d/H$  approaches zero the smooth-unconfined horizontal ceiling jet is reached asymptotically  $\theta_{\max}$  approaches 1. As  $d/H$  increases beyond 0.25,  $\theta_{\max}$  approaches zero which is a no-spillage or corridor flow condition. Furthermore, it has been demonstrated that a relatively flat profile is obtained in the secondary bay as  $d/H$  reaches about 10% value. Thus, determining  $\theta_{\max}$  may be sufficient to characterize the ceiling jet temperature. Although the flow velocity was not measured in this work, previous work [12] indicates a large reduction in velocity in the secondary bay.

Work of Vettori [19] comes closest to large-scale validation test. However, his detailed measurements were limited to 4 locations in a beamed ceiling configuration with 16" beam spacing, plume impinged on several bays and beams and the measurement was at least 4 bays away from the plume impingement. The data graphed in report by Vettori shows general agreement with the predictions using Equation (13). The ceiling height for these experiments was 2.4 m. This type of data can only provide qualitative comparisons and the measurement details can not match small-scale conditions.

## 5. Application Examples

The failure or delay in heat detector or sprinkler actuation jeopardizes the detection and suppression system reliability. It is very important to be able to deter-

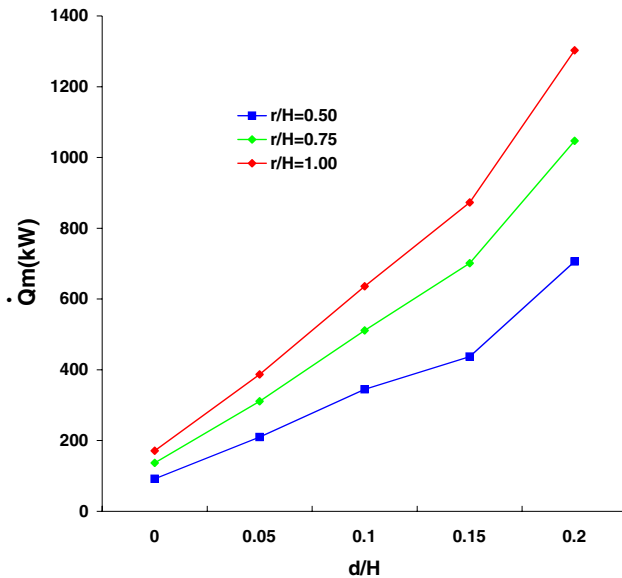


**Figure 12. Calculated minimum fire size needed to actuate a heat detector or sprinkler head placed in the secondary bay.**

mine if the minimum heat release rate required for detector or sprinkler operation exceeds a design threshold fire size for sprinklers or heat detectors positioned in every other bay.

The maximum temperature of ceiling jet within the secondary bay can be used to determine the minimum fire size required for the actuation of each detector or sprinkler based on the developed correlation regardless of  $l_b/H$ . For example, if ceiling height  $H$  is 3.5 m and temperature rating of detector or sprinkler is 57.2°C (135°F), the minimum fire size for different  $d/H$  and  $r/H$  can be calculated. The results of this calculation are plotted in Figure 12. It is shown that with increasing  $d/H$ , the minimum fire size  $\dot{Q}_m$  vs.  $d/H$  rise drastically. The larger  $r/H$ , the steeper is the slope of  $\dot{Q}_m$  vs.  $d/H$ . Furthermore, the minimum fire size under the condition of  $0.03 < d/H < 0.25$  and  $0.25 < r/H < 1.0$  can be predicated on the basis of correlation established in this work, detector or sprinkler's temperature rating and configuration of beamed ceiling.

## 6. Conclusions

This paper established an empirical equation for beamed ceiling jet maximum temperature within the secondary bay (or channel) as a function of the ratio of the beam depth to ceiling height and the position along the secondary bay axis. It is obvious that for  $d/H > 0.20$ , the non-dimensional maximum temperature decreases dramatically, and the flow within the bay approaches a corridor flow. There is, on the average, 15–90% reductions in the temperature of ceiling jet within secondary channels for the beam depths of 3–25% of ceiling height, respectively, when compared with the smooth horizontal unconfined case. This equation was demonstrated for its practical application to determine the minimum fire size detected by a heat detector placed in a secondary channel. The experimental data in this work may be used to validate the numerical results generated by field models. The data and correlation developed here can also be used to perform parametric studies of ceiling geometry effects on smoke and heat detector performance. The results reported here are limited to those cases when the fire plume impinges the ceiling within the primary bay and the flame height is considerably less than the ceiling height. The  $\dot{Q}^*$  range is large enough to include practical fire sizes, however, the relation to the smooth horizontal ceiling correlation limits its validity to  $r/H = 1.0$  with the added caveat that this correlation was developed using small-scale experiment within a weak-plume range. Although, there is an advantage as early detection of growing fires often falls within very small fires and weak plume region.

## Acknowledgments

This work was sponsored, in part, by the Educational and Scientific Foundation, Society of Fire Protection Engineers. The financial support for this work is greatly appreciated.

## References

- [1] H. Baum and K. McGrattan, "Simulation Enclosure Fire Dynamics and Suppression". *National Institute of Standards and Technology, National Research Institute of Fire and Disaster (NRIFD) Symposium, 2nd Proceedings*. July 17–19, 2002, Tokyo, Japan, pp. 217–233.
- [2] G.P. Forney, R.W. Bukowski, and W. D. Davis, "Simulating the Effect of Flat Beamed Ceiling on Detector and Sprinkler Response". American Society of Mechanical Engineers. in S. Acharya, K. Annamalai, C. Presser, and R.D. Skocypec (eds.), *Fire, Combustion, and Hazardous Waste Processing*. HTD-vol. 296. American Society of Mechanical Engineers, Chicago IL NY, 1994, pp. 143–150.
- [3] NFPA 13., *Standard for the Installation of Sprinkler Systems*, National Fire Protection Association, Quincy, MA, 2002.
- [4] NFPA 13D., *Installation of Sprinkler Systems in One and Two-Family Dwellings and Manufactured Homes*, National Fire Protection Association, Quincy, MA, 2002.
- [5] NFPA 72., *National Fire Alarm Code*, National Fire Protection Association, Quincy, MA, 2002.
- [6] G. Forney, W. Davis, and J. Klote, *Simulating the Effect of Beamed Ceilings on Smoke Flow, Part I. Comparison of Numerical and Experimental Results*, NISTIR 4994, NIST, Dec., 1992.
- [7] G. Heskestad, *Model Study of ESFR Sprinkler Response Under Beamed Ceilings. Technical Report, FMRC J.I.0N0E3.RU*, Factory Mutual Research Corporation, Norwood, MA, 1987.
- [8] R. Bill Jr., H.-C. Kung, W. Brown, and E. Hill, "Effects of Cathedral and beamed Ceiling Construction on Residential Sprinkler Performance. Fire Safety Science", in *Proc of the Third Int'l Symposium*, Elsevier Pub, 1988, pp. 643–653.
- [9] G. Heskestad and M. Delichatsios, *Environments of Fire Detectors – Phase I: Effect of Fire Size, Ceiling Height and Material. Technical Report, FMRC Serial No 22427*, Factory Mutual Research Corporation, Norwood, MA, May 1977.
- [10] G. Heskestad and M. Delichatsios, *Environment of Fire Detectors – Phase II: Effect of Ceiling Configuration, FMRC, No 22584*, Factory Mutual Research Corp., 1978.
- [11] M. Delichatsios, "The Flow of Fire Gases Under a Beamed Ceiling", *Combustion and Flame*, vol. 43, 1981, pp. 1 .
- [12] C. Koslowski and V. Motevalli, "Effect of Beams on Ceiling Jet Behavior and Heat Detector Operation", *Journal of Fire Protection Engineering*, vol. 5(3), 1993, pp. 97–112.
- [13] J. Quiniere, "Scaling Applications in Fire Research", *Fire Safety Journal*, vol. 15, 1989, pp. 3–29 Elsevier Science.
- [14] V. Motevalli, *Characterizing the Unconfined Ceiling Jet Under Steady State Conditions*. PhD Dissertation, University of Maryland, 1989.
- [15] V. Motevalli and C. Marks, "Characterizing the Unconfined Ceiling Jet Steady-State Conditions: A Reassessment", in *Fire Safety Science Proceedings of the 3rd International Symposium*, Elsevier Pub Co, Inc, 1991, pp. 301–312.
- [16] Z. Yuan, *Study of a Ceiling Jet Induced by Steady Fire Source under an Unconfined Ceiling with Beams*. MS thesis, Worcester Polytechnic Institute, May 1994.
- [17] C. Koslowski and V. Motevalli, "Behavior of a 2-Dimensional Ceiling Jet Flow: A Beamed Ceiling Configuration". in T. Kashiwagi (ed.), *Fire Safety Science – Proc of the Fourth Int'l Symposium*. International Assoc of Fire Safety Sci, 1994, pp. 469–480.

- [18] User's manual, Math/Library, Fortran Subroutines for Mathematical Applications Softcover Edition 1.1, IMSL, Problem-Solving Software System, p. 835, Jan 1989.
- [19] R. Vettori, "Effect of an Obstructed Ceiling on the Activation Time of a Residential Sprinkler". National Institute of Standards and Technology, NISTIR 6253, November 1998.